Journal of Vacuum Science and Technology A

RESEARCH ARTICLE | DECEMBER 28 2023

Apparatus design of operando hydrogen microscope for visualization of time-dependent distribution of hydrogen

Naoya Miyauchi ; Taro Yakabe ; Yoshiharu Murase; Masahiro Kitajima ; Shoji Takagi; Akiko N. Itakura

J. Vac. Sci. Technol. A 42, 013201 (2024)
https://doi.org/10.1116/6.0003153

JVST A
Journal of Vacuum Science & Technology A

ARTICLE

pubs.aip.org/avs/jva

Apparatus design of operando hydrogen microscope for visualization of time-dependent distribution of hydrogen

Cite as: J. Vac. Sci. Technol. A 42, 013201 (2024); doi: 10.1116/6.0003153
Submitted: 20 September 2023 · Accepted: 20 November 2023 ·
Published Online: 28 December 2023

Naoya Miyauchi,[1,a)] Taro Yakabe,[1] Yoshiharu Murase,[1] Masahiro Kitajima,[1] Shoji Takagi,[2] and Akiko N. Itakura[1]

AFFILIATIONS

[1]National Institute for Materials Science, 1-2-1 Sengen, Tsukuba-shi, Ibaraki 305-0047, Japan
[2]Department of Physics, Toho University, 2-1-1 Miyama, Funabashi-shi, Chiba 274-8510, Japan

[a)]**Author to whom correspondence should be addressed:** Miyauchi.Naoya@nims.go.jp

ABSTRACT

The operando hydrogen microscope is an original apparatus that has been developed to visualize the time-dependent permeation of hydrogen through a sample. This apparatus is developed based on an ultrahigh vacuum scanning electron microscope (UHV SEM). The system consists of a lens system to focus ions produced by electron-stimulated desorption (ESD), an ion detector optimized for ESD-signal detection, and a two-dimensional measurement program synchronized with the position information of the electron beam. The developed detectors and electrostatic lenses enable highly sensitive detection of the ions. In this paper, we show the details of the instrumentation of the operando hydrogen microscope. We have succeeded in recording hydrogen and deuterium flowing from the rear of metals to the surface as a series of time-lapse images, showing the time-dependent changes in the surface distribution of hydrogen and deuterium. Deuterium permeation through the metal sample was dynamically visualized at the surface by the two-dimensional mapping of the desorbed ions induced by scanning electron beam irradiation.

I. INTRODUCTION

Visualization of hydrogen is of great interest in the fields of vacuum science technology and structural materials' development. Hydrogen is the main component of residual gases in a vacuum chamber under ultrahigh vacuum (UHV). This is because hydrogen within the material of the container is released into the vacuum. The outgassing has been reduced by using new materials and surface treatment techniques such as inner-surface polishing,[1] coatings,[2–4] and surface oxidation treatment.[5] These improvement techniques for the suppression of outgassing have been assessed as an average of all outgassing from all surfaces. However, some surfaces could have local outgassing points that would be overlooked when using such macroscopic evaluation methods.[6] We consider it important to know not only the quantity of hydrogen outgassing but also the position at which the outgassing occurs.

Metal structural materials are key components in infrastructures that must withstand harsh conditions. In recent years, materials for hydrogen stations have become increasingly important. The mechanical properties of metal structural materials deteriorate with hydrogen embrittlement as well as corrosion, leading to possibly extremely dangerous situations. There are several structural materials that are suitable for use under hydrogen environments and approved for use. Stainless steel is one of such metal materials, being an alloy that contains only a small amount of hydrogen in the material that does not easily cause the hydrogen embrittlement.

However, the phenomenon of hydrogen diffusion and embrittlement is not fully understood. This seems to be one of the most difficult aspects of the problem. Hydrogen atoms within a diffusion channel and at trapping sites cannot be identified directly, and it is even more difficult to directly catch the diffusion dynamics of hydrogen with real-time observations. For example, hydrogen cannot be observed by Auger electron spectroscopy, which is the technique for measuring the surface composition. The thermal desorption method can measure the amount of hydrogen, but it

TABLE I. Differences between hydrogen visualization in ESD.

	Joshi[14]	Poppa[15]	Takagi[16]	Ueda[17]	This work
Imaging	Yes	Yes	Yes	Yes	Yes
Spatial resolution	3 μm	5 μm	1 μm	700 nm	1 μm
Mass selects	SIMS analyzer	QMS	Not use (CMA)	Time-of-flight	Not use (CMA)
Detection efficiency	Low	Low	Low	Low	High
Hydrogen permeation detection	No	No	No	No	Yes
Hydrogen supply	No	From measurement surface	From measurement surface	From measurement surface	Sample backside (or from measurement surface)

provides neither location information nor time-related information. Visualization of the local distribution of hydrogen on a surface has been attempted by several methods, including a hydrogen microprint technique,[7] secondary ion mass spectrometry (SIMS),[8] Kelvin probe force microscopy,[9] and tritium autoradiography.[10] Although particularly SIMS provides positional information, it is a destructive method performed while milling the sample. So, the reproducibility of the data obtained cannot be investigated. For this reason, we do not obtain convincing information on the locations where the hydrogen involved in hydrogen embrittlement exists. To solve this problem, we need a nondestructive and dynamic method to directly observe the behavior of hydrogen.

When the surface of a solid is irradiated with photons or electrons, atoms and molecules on or near the surface are electronically excited. As a result of the relaxation process, they are released from the surface as ions and neutral particles. This is generally referred to as desorption induced by electron transitions (DIETs). When electrons are used as an excitation source, it is called electron-stimulated desorption (ESD) [and in the case of photons, photon-stimulated desorption (PSD)]. ESD has become one of the major methods for surface analysis because the desorbed ions provide information on the bonding and orientation of adsorbates. The Menzel–Gomer–Redhead (MGR) model[11,12] was proposed as a theoretical explanation of the ESD mechanism where the electrons excite the adsorbed atoms and release them from their bonding orbitals as ions via the antibonding orbitals. Although this model has successfully explained many experimental results, it is not able to explain all of them and, therefore, Antoniewicz proposed an extended MGR model[13] in which the ions produced by electronic excitation are desorbed via the ionization-bound state. However, if it is a metal sample and it is thought that ESD phenomena according to the MGR model will occur, the ESD map can be regarded as the distribution of surface atoms and surface adsorbed atoms. ESD studies to date have mainly focused on surface reactions, measured the angular distribution of the desorbed ion, and analyzed a variety of ions using a TOF mass spectrometer (not visualization). The first imaging of ESD was performed more than 40 years ago.[14,15] Not many papers were published over the next 20 years.[16,17] Our apparatus is unique in that it focuses exclusively on hydrogen and the 2D distribution, and that it incorporates hydrogen in the permeation type for materials research. By focusing on hydrogen permeation and incorporating permeation measurements from the back side, we were able to expand the scope of use of ESD techniques to the study of the interior of materials rather than studying their surfaces. In addition, although previous apparatuses had produced good results, the detection efficiency of ESD ions is generally not high; so in order to elucidate the behavior of adatoms, it is necessary to supply them to the sample surface. Usually, it was supplied in the measurement chamber on the surface side of the sample. The experimental conditions were difficult for hydrogen, as its partial pressure in ultrahigh vacuum is hard to control. The differences between each apparatus are summarized in Table I.

The advantage of this apparatus is that its ion detection efficiency is an order of magnitude higher than other apparatuses. The method of supplying hydrogen also differs.

Our group is the first to apply a scanning electron beam to the visualization of permeating hydrogen[18–21] in real time. We have reported on the distribution of hydrogen on the surface of the metal using our original hydrogen measurement system equipped with a continuous supply of hydrogen to the rear of the sample.[18–21] The distribution of visualized hydrogen reflected the microscopic structures of crystal grains in stainless steel (SUS304) that had been observed by SEM and electron backscattered diffraction (EBSD). From the evaluation of the time-dependent permeation of hydrogen through each crystal grain, we were able to obtain the local diffusion coefficient for each grain.[21] The role of a Cr_2O_3 coating, a treatment applied to inhibit the adsorption of hydrogen, was also evaluated, and local hydrogen outgassing through small defects in the coating was confirmed in the ESD images.[6]

In this paper, we report the details of the equipment design we used for hydrogen visualization (named the operando hydrogen microscope) and the detailed experimental processes for visualization using the system.

II. OVERVIEW OF OPERANDO HYDROGEN MICROSCOPE AND ORIGINAL DETECTOR DESIGN

The operando hydrogen microscope is our developed experimental apparatus, which consists of a hydrogen detection system by ESD and a gas phase hydrogen supply system to a sample. The hydrogen detection system is based on an UHV SEM. Therefore, the spatial resolution is dependent on the electron beam source of the SEM instrument. The apparatus we have developed is based

around a tungsten filament SEM (JAMP10; JEOL Co.). Generally, the optimal energies of the incident electron for the ionization of adsorbed atoms are several 100 eV.[22] To achieve a high spatial resolution of 1 μm, we use an electron energy of 1–2 keV (which is a sufficient ESD ionization efficiency[22]).

A schematic of our experimental setup is shown in Fig. 1(a). Here, we describe a general aspect of the design and the experimental conditions. A hydrogen supply line with sample, an ESD ion detector, and a quadrupole mass spectrometer (QMG220; Pfeiffer) are added into the measurement chamber of the commercially available UHV-type SEM. The sample holder with hydrogen supply is positioned in the center of the measurement chamber and is connected to the gas supply system. The base pressure of hydrogen gas supply system is maintained at 2×10^{-4} Pa by turbomolecular pump 1(TMP1) (HiPace 80; Pfeiffer).

In the first experiment, our sample holder had the sample attached by welding. However, we made several improvements to the sample holder so that experiments can be performed with other materials. Figure 1(b) shows the metal O-ring specifications that are compatible with thin film samples. A Faraday cup was prepared near the sample to measure the current value of the scanning electrons used for ESD. For soft samples that cannot withstand the tightness of a metal O-ring, we seal with an elastomer O-ring made of fluorocarbon rubber [Fig. 1(c)]. Since there is a possibility of hydrogen leakage with the O-rings, we use double O-rings. The space between two O-rings is maintained by differential pumping with TMP1.

We have designed an ion detector and electrostatic lens using ion optics to achieve both high sensitivity and high resolution. We have tried several ion detectors, including multiple ion multipliers such as multichannel plates (F4655-14; Hamamatsu Photonics K.K.) and Channeltron (4821; Photonis USA Inc.), and electrostatic lens for ion focusing. The electrostatic lens is set near the sample in order to direct ESD ions to the entrance of the detection system. The measurement chamber is maintained at 1×10^{-7} Pa by a TMP2 (MITSUBISHI PT-500-A300) and an ion pump (PUT-3; ULVAC). During hydrogen measurements, TMP2 is shut off and only the ion pump is used. Gases that can be used include not only hydrogen but also helium, oxygen, and other gases, as well as water. Hydrogen or deuterium gas can be supplied at a maximum of 0.3 MPa. The sample temperature is set by a noncontact halogen lamp (10.8 V, 30 W; Toshiba) attached to the rear of the sample (hydrogen supply side) that can maintain the sample at a constant temperature from room temperature to about 600 K. The sample temperatures were measured by using thermocouples (T type) and controlled by a digital proportional-integral-differential controller (KP-1000C; Chino). For samples with low thermal conductivity, such as stainless steel, a P.I.D. controller was used to keep the sample temperature constant. (e.g., sample temperature 473 ± 0.1 K)

The surface structure of the sample is acquired as a monochrome image from the SEM image drawn by scanning electron beams. In the ESD ion images, the electron beam scanning signals are acquired as transistor-transistor logic (TTL) signals by a program that we made ourselves using LabVIEW (National Instruments), and the electron irradiation time per image is 400 s. After that, a margin of 50 s is allowed for formatting and exporting the stored data. The scanning speed of the electron beam can be changed.

An electron multiplier is used for the detection of hydrogen ions. The ion detected by an electron multiplier is electronically

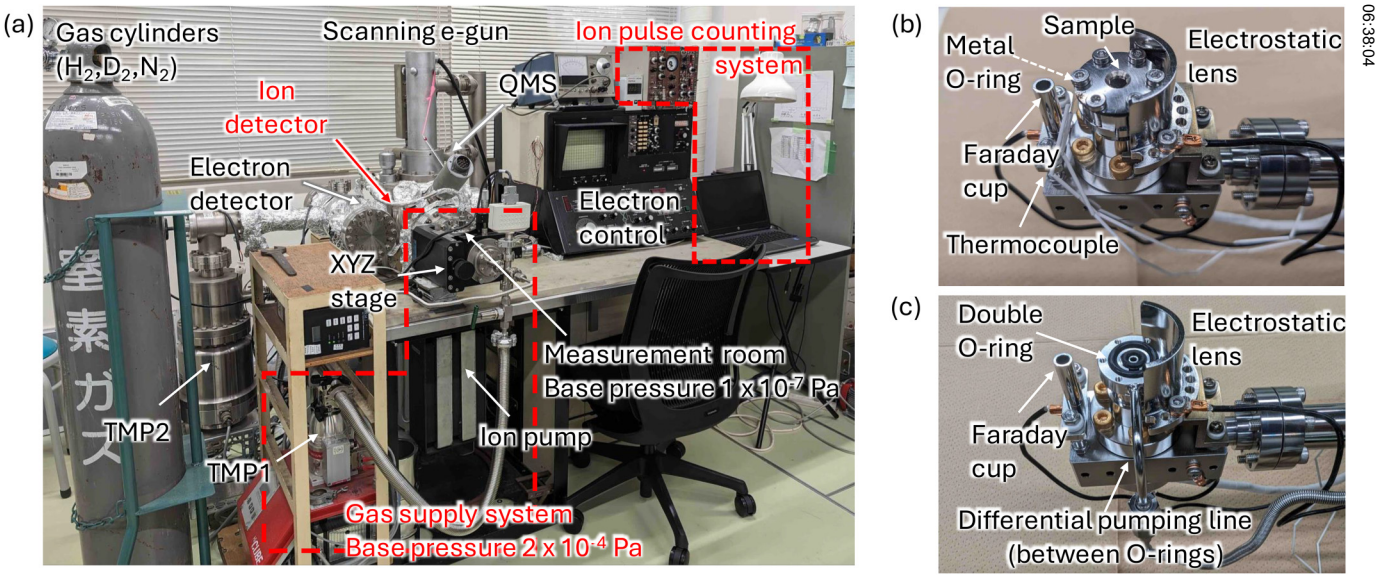

FIG. 1. Frontal view of the operando hydrogen microscope. (a) Operando hydrogen microscope is based on an ultrahigh vacuum SEM. Added systems are mentioned in red. (b) Metal O-ring-type sample holder incorporating a dedicated gas supply system is added in the measurement chamber. (c) Double O-ring-type sample holder. A conventional secondary electron detector, a highly efficient lens system for ion focusing, and an ion detector are equipped in the measurement chamber.

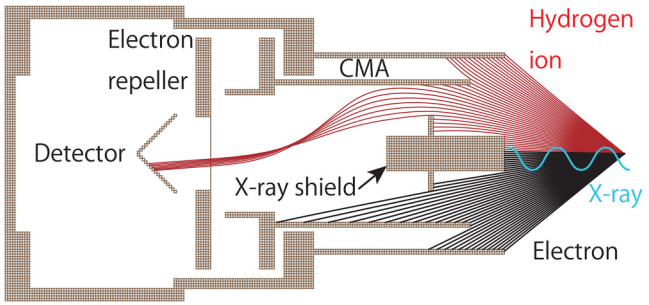

FIG. 2. Simulation of the designed ion detector for removing scattered electrons. The simulation was performed by using SIMION7.0. The mesh size in the figure is simulated as 0.5 mm/mesh. Red line, trajectory of hydrogen ions; black line, trajectory of scattered electrons.

amplified to a large amplitude, and the output as a negative pulse wave is about −10 to −20 mV. The signals are amplified through a high-speed preamplifier and amplifier and are sorted by a single channel analyzer and output as a TTL signal. This is the most commonly used method for pulse counting detection of ions (e.g., in time-of-flight mass spectrometry).

The system consists of a combination of lens systems that only focus ions while excluding scattered electrons and soft x rays. Soft x rays are produced when a metal sample is irradiated with an electron beam. Since the soft x rays cannot be distinguished from the ion signal when they reach the detector, at the entrance of the detector is placeda lens system that comprises a cylindrical mirror analyzer (CMA) is placed at the entrance of the detector. The shield not only excludes soft x rays but also efficiently focuses the ion on the detector. The lens system includes a repeller to exclude scattered electrons caused by the scattering of the incident electron beam. We performed a simulation to determine the shape of the electrostatic lens by using charged particle trajectory calculation software SIMION 7.0 (Scientific Instrument Services, Inc.), which can apply an arbitrary voltage to the electrodes and obtain equipotential surfaces to obtain the orbits of ions and electrons from arbitrary positions: electron and ion trajectories. Figure 2 shows the trajectories of electrons at 1.0 keV and hydrogen ions at 3 eV. Here, the CMA was charged at 5 V, and to prevent the scattered electrons from entering the detector, the repeller was charged at 1.1 kV. As seen in Fig. 2, the ion detector efficiently collects ions (red line) while removing scattered electrons (black line). Hydrogen ions are well guided into the detector according to the electric field gradient created by the detector, CMA, and repeller.

Adatoms (adsorbed hydrogen) on a surface are ionized and emitted through ESD. Therefore, only ions that are emitted in the direction of the ion detector can be detected; however, their detection efficiency was very low (as is). In order to improve the detection efficiency, our system has an electrostatic lens mechanism around the sample to efficiently guide the isotropically emitted ions, which distribute over a wide angle, to the ion detector. Figure 3 shows the results of simulated hydrogen ion (E = 3 eV) trajectories obtained by SIMION. In order to know the effects of lens' shape and voltages, we simulated the ion trajectories with and without the electrostatic lens. Figure 3(a) is a side view showing the trajectory of the ions emitted spread from the angle q of 0 to p from the surface at the center position of the sample without the electrostatic lens. Figure 3(b) shows the ion trajectory using a 5 V electrostatic lens. The ions in any angle region are known to be

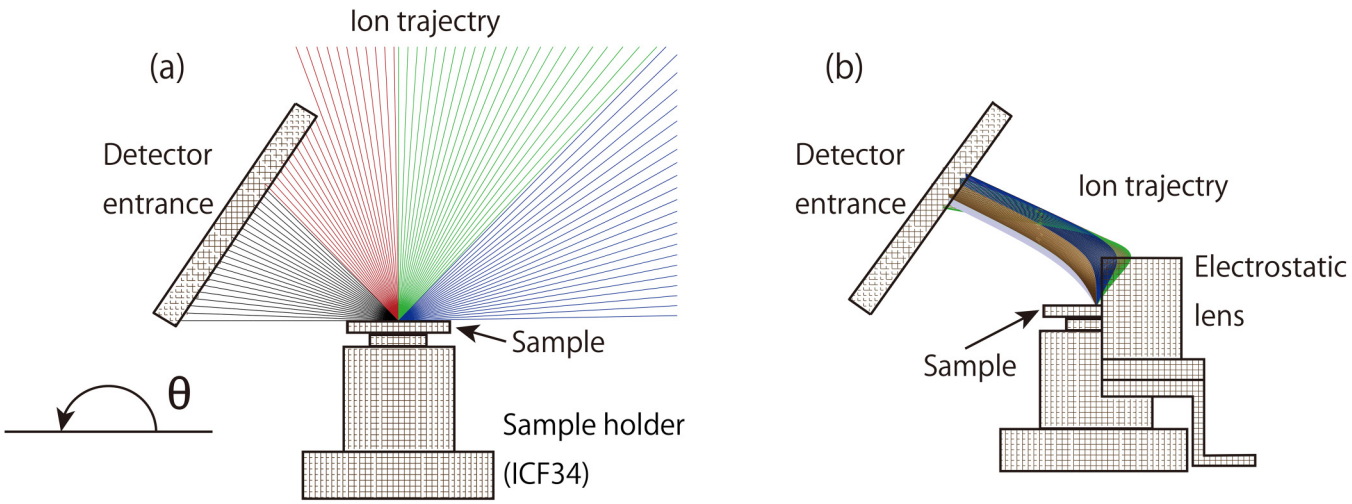

FIG. 3. Hydrogen ion trajectory simulation (side view) without electrostatic lens (a) and with electrostatic lens (b). We used SIMION to optimize the electrostatic lens. The mesh size in the figure is simulated as 0.5 mm/mesh. To demonstrate the effect of the electrostatic lens on the trajectory of the emitted ions, the ion trajectories are divided into four angle regions: blue, 0-p/4; green, p/4-p/2; red, p/2-3p/4; and black, 3p/4-p. (a) Without an electrostatic lens, hydrogen ions are emitted isotropically, and a small amount of the emitted hydrogen ions are countable. (b) With an electrostatic lens, much more hydrogen ions are collected on the direction of the detector.

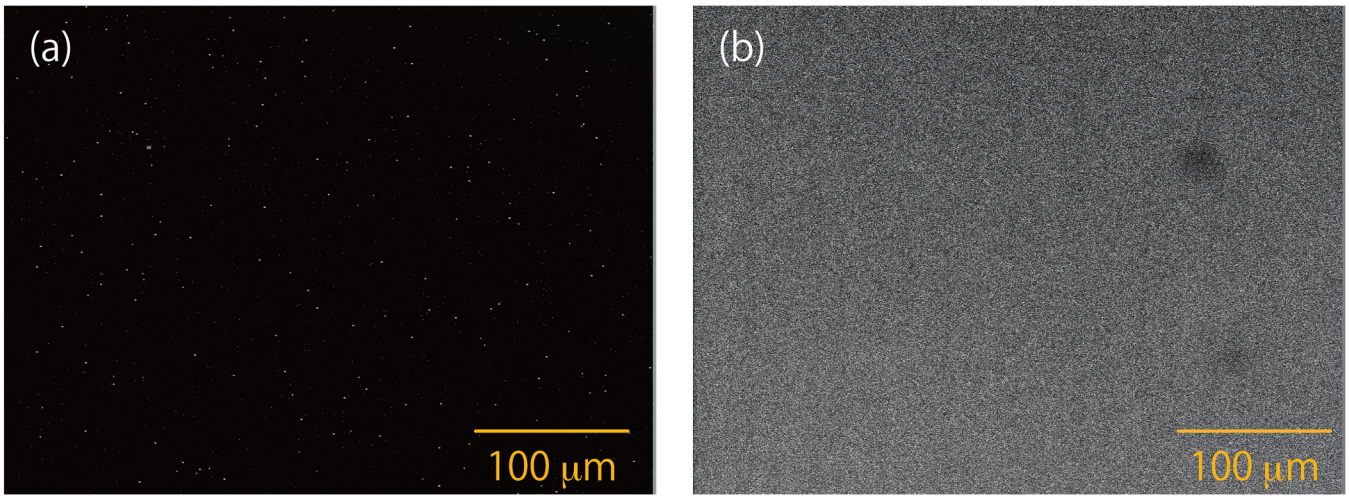

FIG. 4. ESD ion images without electrostatic lens (a) and with electrostatic lens (b). With the electrostatic lens, the number of ions detected increases significantly, resulting in a clearer deuterium image, but without the electrostatic lens, the number of ions in the image is very sparse.

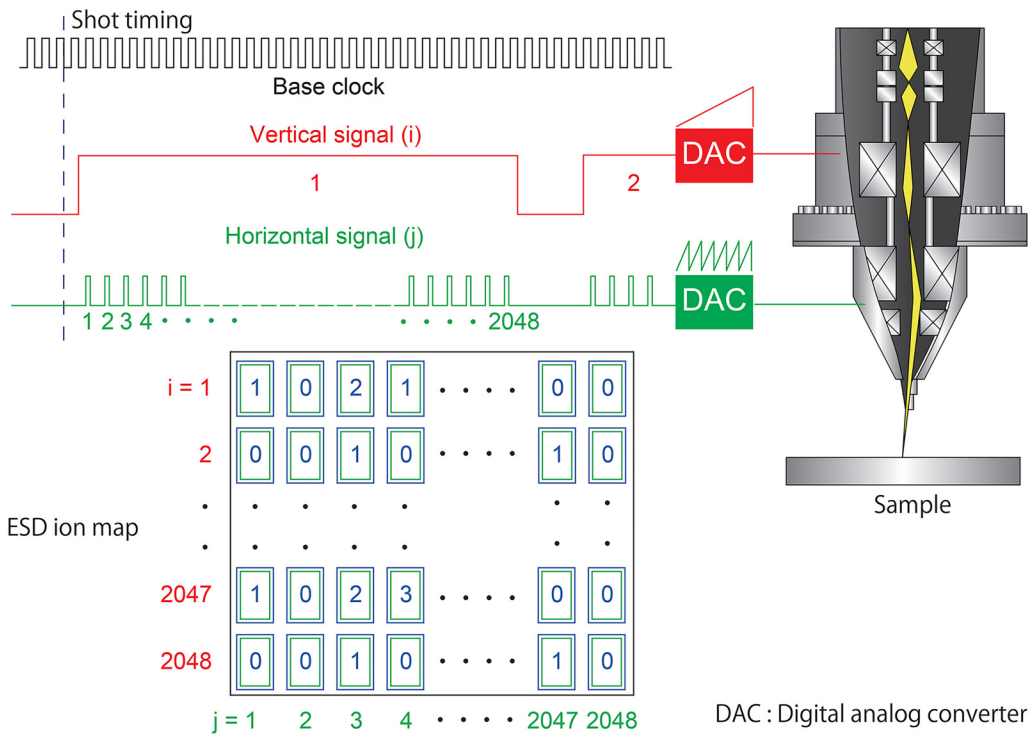

FIG. 5. Scanning electron beam position information and pulse count measurement program. The scanning electron beam is controlled by two coils. The two coils are controlled by TTL based on the base clock. Scanned electron is constructed with 2048 × 2048 pulses for the vertical and horizontal signals. The TTL signals are used to provide vertical and horizontal position information, and the number of ions at each point is used as the ESD ion map.

guided only to the detector. Thus, most of the ions released at a wide angle are guided toward the detector, greatly improving the detection efficiency.

As the simulation suggests, with the electrostatic lens, the emitted hydrogen ions should be well focused toward the detector. We actually tried the signal detection for without and with the electrostatic lens. The number of ion counts was significantly improved from 2926 ion counts per frame with no electrostatic lens to 801 290 ion counts under the same experimental conditions (SUS304, $T = 473$ K, $P_{D2} = 1 \times 10^5$ Pa). The ion signal can be increased about 200 times by using the electrostatic lens. By integrating the surface distribution of hydrogen, the ability to obtain the structure-dependent distribution of permeating hydrogen is dramatically improved, as shown in Fig. 4.

In order to visualize hydrogen, it is important to correlate the positional information of the electron beam with that of the detected ions. We have developed a program to synchronize the ion signal with the scanning electron beam. LabVIEW (National Instruments, Inc.) was used to create the program. The program's synchronization signal is the base clock of the SEM or a TTL signal generated from an external function generator [see Fig. 5]. The SEM scans the electron beam based on this base clock. For example, in the JAMP10 unit that we use, the focus of the electron beam is shifted by driving the vertical and horizontal coils via the digital-analog converter (DAC) for the vertical and horizontal clocks, respectively. The LabVIEW program combines the vertical and horizontal signals to obtain positional information and connects the electron irradiation position to the ion signal. The program first sends a reset signal to the SEM to return the electron irradiation position to the origin. After that, the vertical and horizontal signals that started the measurement are led to the counter in the program, the position information (i,j) is obtained, and the number of ion signals detected at that time is set to $k_{i,j}$ to obtain around one point. For example, to obtain an image of 2048×2048 pixels, the electron beams are scanned by TTL with 2048 vertical scanning signals and 2048 horizontal scanning signals. There are 2048 horizontal signals in a single vertical signal, and the ion count is obtained in synchronization with the horizontal signal. In the first row ($i = 1$), 2048 ch of ion signals $k_{1,1}$, $k_{1,2}$, $k_{1,3}$ … $k_{1,2048}$ are counted. By doing these up to the 2048th row, we save them as text data in a 2048×2048 matrix (Fig. 5).

III. CONFIRMATION OF DEUTERIUM PERMEATION AND TIME EVOLUTION OF DISTRIBUTION

In this chapter, we show that it is possible to measure time developmental distributions of surface deuterium. Deuterium is chemically similar to hydrogen, but it has one more neutron and has a mass number of 2. It is possible to observe permeated deuterium, distinguishing it from residual hydrogen in the chamber. The sample was a stainless steel 304L plate ($t = 100\,\mu$m), which was heat-treated, and 10% cold-rolled plates were prepared after a surface polishing process. Prior to deuterium permeation, the sample was heated to 573 K in the same time chamber baking for 48 h. The permeation measurements were conducted at 473 K in this experiment. The gas supply system is exhausted by TMP1 to 2×10^{-4} Pa. When supplying gas, we shut off TMP1 and supply gas. In this experiment, 1×10^5 Pa (1 atm) of deuterium (99.96%) was supplied.

To compare the time evolution of ESD with conventional deuterium permeation experiments, the desorbed deuterium was compared with that measured by the QMS. The overall shapes of the two deuterium permeations appear similar but in the initial permeation process (see the dashed lined box) in Fig. 6. The ESD ion intensity increases faster than the increase detected by the QMS. This is because ESD directly detects desorbed deuterium ions and ionized single atoms staying on the surface, while QMS detects thermally desorbed deuterium molecules through two deuterium atoms' recombination.

Permeation experiments were conducted for about 65 h after exposure to deuterium. Figure 7 shows the time evolution with deuterium exposure from time = 0 to 65 h. A single ESD ion map does not produce an ion image that corresponds to the shape of the grains. Because of the low permeation of deuterium through the stainless steel, sufficient ions are not obtained to get a clear ESD image of the grain structure. The images shown here are the images integrated every 5 h.

After a few hours of exposure to deuterium gas, the number density of the ESD ions increased, resulting in a gradual increase in the brightness of the entire surface image. It can be seen that the distribution of deuterium does not uniformly increase with time over the entire surface but that the ESD ion density appears

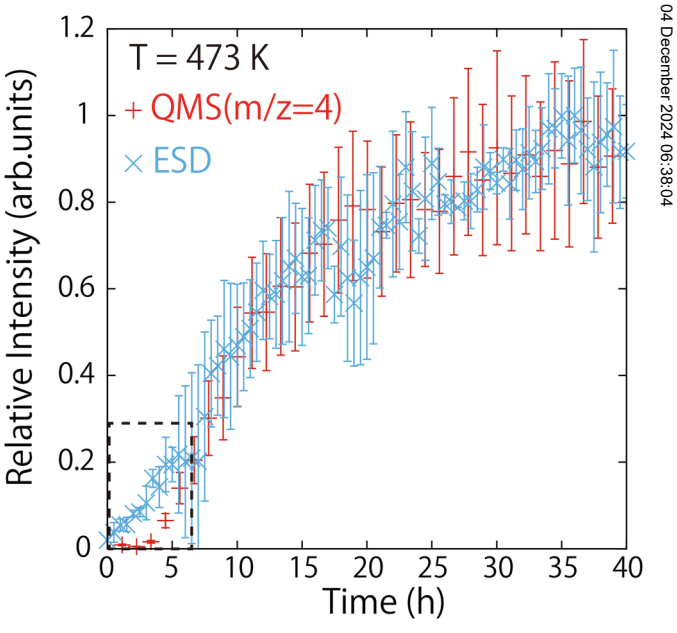

FIG. 6. Deuterium permeation of the SUS304 sample measured by QMS and ESD. The QMS data are the ion current at m/z = 4, and the ESD data are the ion count for one image. These were normalized by values over 35 h, when the time variation in the signal was smaller for comparison. In the case of QMS, the signal starts to increase about 3 h after exposure, while in the case of ESD, the signal increases immediately after exposure. The dashed line box indicates the initial permeation.

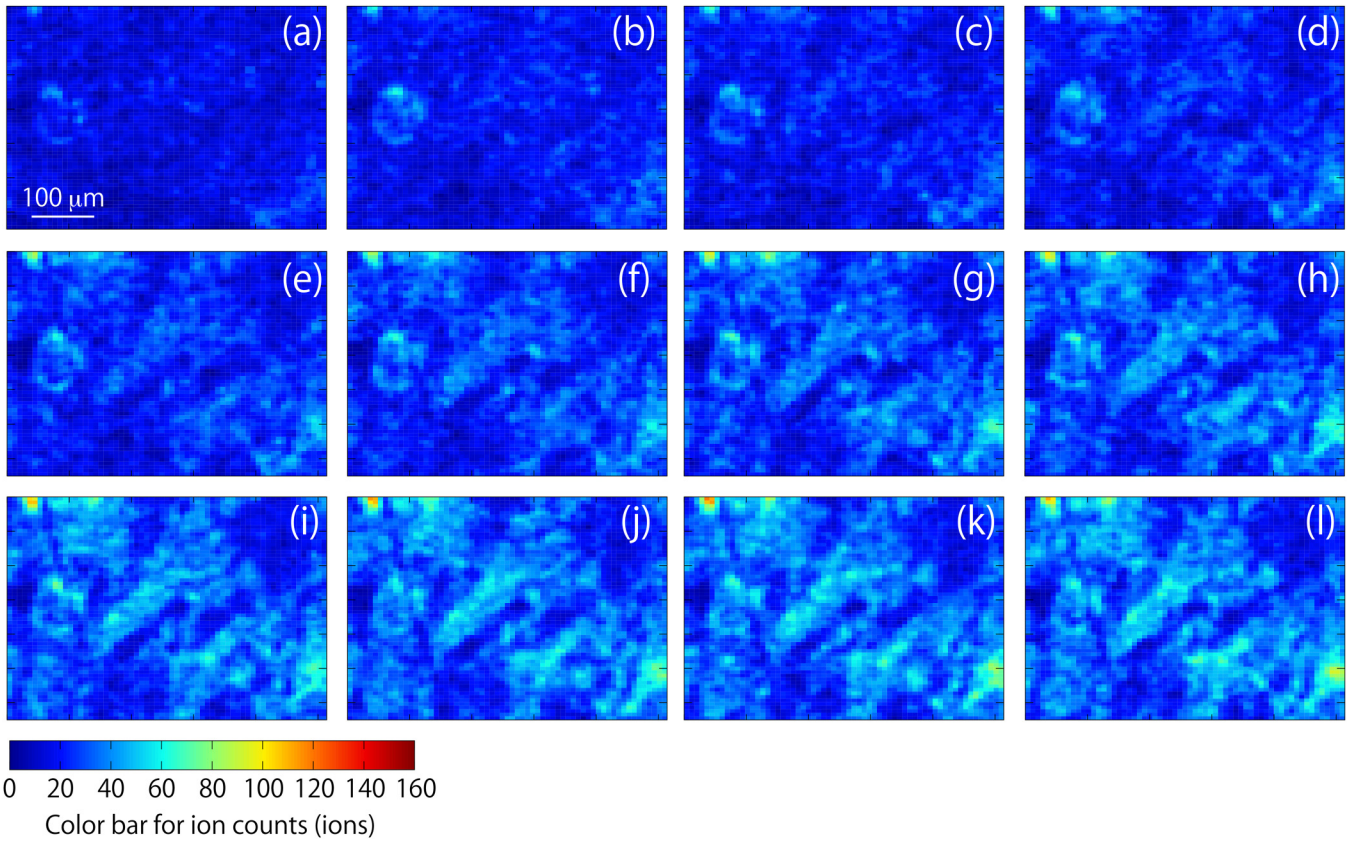

FIG. 7. Time variation of visualized deuterium permeation. Evolution of the permeated deuterium in the five hourly integrated ESD maps, (a) 0–5 h, (b) 10–15 h, (c) 15–20 h, (d) 20–25 h, (e) 20–25 h, (f) 25–30 h, (g) 30–35 h, (h) 40–45 h, (i) 45–50 h, (j) 50–55 h, (k) 55–60 h, and (l) 60–65 h, acquired after exposure to deuterium. The size of all ESD maps is 520 × 340 mm^2.

depending on the location. Comparing the ESD map of deuterium ions with that of the SEM image taken at the same position of the sample, we found that the shapes and locations for most of the bright ESD areas are the same as those for SEM. We have also confirmed this by EBSD observations.[19]

As in this paper, many researchers replace deuterium with hydrogen in their experiments when studying materials and hydrogen. However, it has recently been discussed that known simple isotopic relationships may not be sufficient to fully elucidate the diffusion and permeation behavior of deuterium and hydrogen. We have reported the experimental results using deuterium to mitigate the effects of residual gases. However, in the early experiments in the development of the operando hydrogen microscope, measurements were made using both gases, comparing deuterium permeation with hydrogen permeation. We had compared the total amount of permeation—not local permeation, but the total amount of hydrogen ions or deuterium ions emitted from one frame of approximately 300 × 500 μm^2 area on the stainless steel membrane [Figs. 8(a) and 8(b)].

Since deuterium has a smaller diffusion coefficient[23] than hydrogen, a square root 2 relationship appears as an isotope effect.[24,25] This was as expected. However, within 2 h of the start of the permeation measurement, it deviated from the value of square root 2. As shown in Fig. 6, this time region (0-2h) cannot be measured in QMS. It can be said, only at this grain boundary diffusion, that a phenomenon different from the predicted isotope effect appears. We also considered from previous research that hydrogen was not permeating inside the grain but rather through the grain boundaries at initial 2 h.[19]

In the operando hydrogen microscope, which measures ESD hydrogen (or deuterium) ions, the number of ions desorbed results from the following: (1) hydrogen (deuterium) adsorption on the gas supply side surface of the sample, (2) hydrogen dissolution into the sample material [this depends on the solubility of hydrogen (or deuterium) in the material], (3) diffusion in the material, (4) gushing out of the sample to the measurement side, and (5) desorption as ions by electron stimulation. The number of atoms on the surface measured by (6) ESD is the remaining atoms after some atoms have recombined with neighboring atoms and desorbed as hydrogen (or deuterium) molecules. The molecules can desorb depending on the lateral mobility of atoms due to surface diffusion. It is difficult to identify where and how the

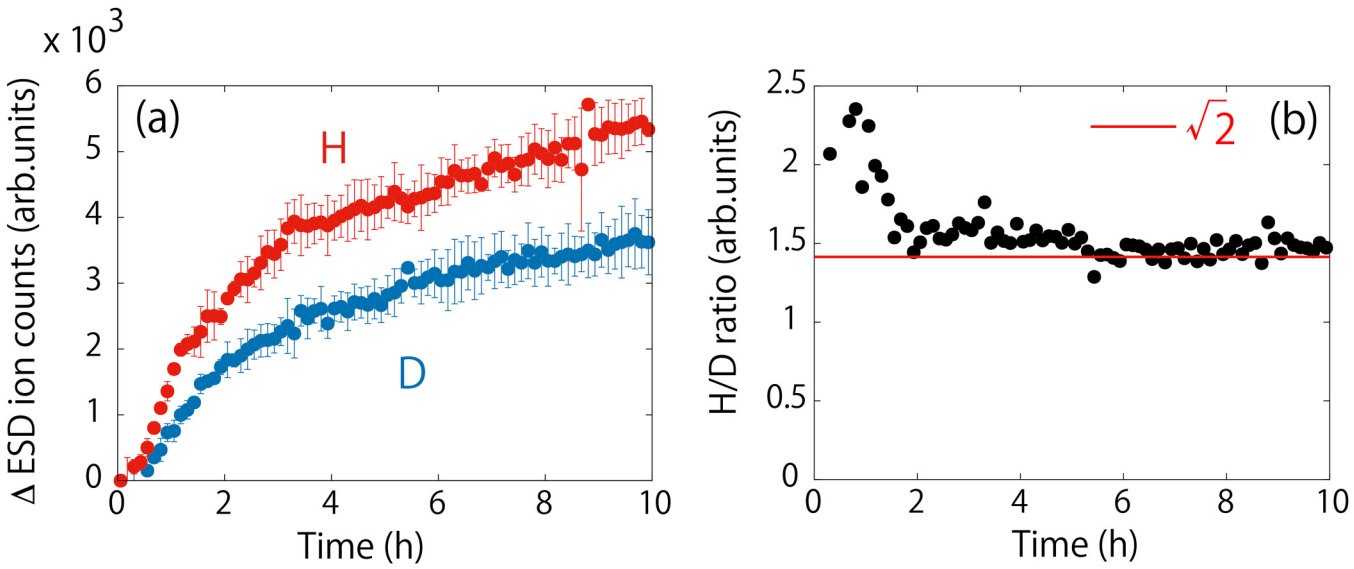

FIG. 8. Difference between hydrogen and deuterium permeation. (a) Time evolution of ion counts of permeated hydrogen (H) and deuterium (D), under the same condition (the same sample and same area, gas pressure of 2.53×10^5 Pa, sample temperature of 573 K). Hydrogen exhibits faster permeation with a larger permeation quantity. (b) Ratio of ion counts vs time. The red line is square root 2 line.

observed deviation from the isotope effects depend on these factors. If we could refer to the experimental results of tritium permeation, we might be able to explain the deviation from the isotope effects.

Only the operando hydrogen microscope can measure individual diffusion at the initial stages of permeation or at each grain or grain boundary. We find that no strong evidence of isotope effects for each permeation pathway is currently available in the literature studies, and we believe that the operando hydrogen microscope can be used in future studies of more detailed hydrogen diffusion phenomena, including isotope effects.

IV. CONCLUSIONS

We have developed a system that allows the visualization of hydrogen (or deuterium) in a dynamic environment. The apparatus supplies hydrogen (or deuterium) from behind the sample and measures the evolution of hydrogen and deuterium through the metal sample. This method enables operative long-time measurements of permeation phenomena, which are not possible with the conventional precharging of hydrogen. This equipment comprises an original ion detector and an ion focusing system in an ultrahigh vacuum SEM, making it possible to detect and visualize deuterium permeation by the ESD mechanism. In the examples we have presented here, deuterium was exposed to the rear surface of the stainless steel and the distribution of the deuterium permeating through the sample was observed. The obtained microscopy results demonstrated that deuterium permeation from individual grains of the sample correlates their crystal structures. By integrating ESD as well as SEM and EBSD, we have been able to gain a microscopic understanding of deuterium permeation in metals. We are able to combine the visualized time-dependent deuterium diffusion with microstructural analysis, having an ability to derive the local diffusion coefficient from individual grains (structures) of the sample, which is not possible with conventional methods of space-average for hydrogen permeation. For further applications, we have reported the effects of point defects on the permeation that could not be evaluated by SEM alone and was also visualized for the special resolution.[6]

The current operando hydrogen microscope uses a tungsten filament and has a spatial resolution of about 1 μm. It is possible to improve the spatial resolution by incorporating the same system into a higher performance SEM (e.g., field emission filament), and we are currently developing such a system.

ACKNOWLEDGMENTS

We thank Daisuke Fujita, Kazutaka Mitsuishi, and Chikashi Nishimura of the National Institute for Materials Science (NIMS), Tetsuji Goto of Toho University and Kenichiro Hirata and Shinji Suzuki who were the students of Toho University. This research was supported by a MEXT/JSPS KAKENHI grant (Grant Nos. JP 22560709, 21H01606, and 22K04935) and under the auspices of the NIFS Collaboration Research program (Nos. NIFS15KEMF052 and NIFS16KEMF052).

AUTHOR DECLARATIONS

Conflict of Interest

The authors have no conflicts to disclose.

Author Contributions

Naoya Miyauchi: Data curation (equal); Formal analysis (equal); Funding acquisition (supporting); Investigation (equal); Methodology (equal); Project administration (supporting); Software (lead); Supervision (equal); Validation (equal); Visualization (equal); Writing – original draft (lead); Writing – review & editing (equal). **Taro Yakabe:** Formal analysis (supporting); Writing – review & editing (equal). **Yoshiharu Murase:** Resources (equal). **Masahiro Kitajima:** Writing – review & editing (equal). **Shoji Takagi:** Conceptualization (equal); Formal analysis (equal); Funding acquisition (equal); Investigation (equal); Methodology (equal); Project administration (equal); Supervision (equal). **Akiko N. Itakura:** Conceptualization (equal); Funding acquisition (equal); Investigation (equal); Methodology (equal); Resources (equal); Supervision (equal); Writing – review & editing (equal).

DATA AVAILABILITY

The data that support the findings of this study are available from the corresponding author upon reasonable request.

REFERENCES

[1]REFERENCESN. Yoshimura, T. Sato, S. Adachi, and T. Kanazawa, J. Vac. Sci. Technol. A **8**, 924 (1990).
[2]Y. Ishikawa and V. Nemanič, Vacuum **69**, 501 (2003).
[3]Y. Ikeda, K. Saitoh, S. Inayoshi, and S. Tsukahara, J. Vac. Soc. Jpn. **37**, 232 (1994).
[4]A. N. Itakura, M. Tosa, S. Ikeda, and K. Yoshihara, Vacuum **47**, 697 (1996).
[5]A. N. Itakura, M. Tosa, Y. Yakabe, N. Miyauchi, A. Kasahara, T. Miyata, and T. Shindo, Vac. Surf. Sci. **61**, 675 (2018).
[6]N. Miyauchi, T. Iwasawa, T. Yakabe, M. Tosa, T. Shindo, S. Takagi, and A. N. Itakura, Appl. Surf. Sci. **492**, 280 (2019).
[7]T. E. Pérez and J. Ovejero Garcia, Scr. Metall. **16**, 161 (1982).
[8]O. Sobol, F. Straub, T. Wirth, G. Holzlechner, T. Boellinghaus, and W. E. S. Unger, Sci. Rep. **6**, 19929 (2016).
[9]C. Larignon, J. Alexis, E. Andrieu, L. Lacroix, G. Odemer, and C. Blanc, Electrochim. Acta **110**, 484 (2013).
[10]C. B. Gilpin, D. H. Paul, S. K. Asunman, and N. A. Tiner, Amer. Soc. Test. Mater., Spec. Tech. Publ. **396**, 7 (1966).
[11]D. Menzel and R. Gomer, J. Chem. Phys. **41**, 3311 (1964).
[12]P. A. Redhead, Can. J. Phys. **42**, 886 (1964).
[13]P. R. Antoniewicz, Phys. Rev. B **21**, 3811 (1980).
[14]A. Joshi and L. E. Davis, J. Vac. Sci. Technol. **14**, 1310 (1977).
[15]H. Poppa and E. Bauer, Surf. Sci. **97**, L309 (1980).
[16]S. Takagi and T. Goto, Surf. Sci. **287–288**, 361 (1993).
[17]Kazuyuki Ueda, Ken'ichi Ishikawa, and Masamichi Yoshimura, Appl. Surf. Sci. **159–160**, 201 (2000).
[18]N. Miyauchi, S. Suzuki, S. Takagi, T. Gotoh, Y. Murase, and A. N. Itakura, J. Vac. Soc. Jpn. **58**, 387 (2015).
[19]N. Miyauchi, K. Hirata, Y. Murase, H. A. Sakaue, T. Yakabe, A. N. Itakura, T. Gotoh, and S. Takagi, Scr. Mater. **144**, 69 (2018).
[20]T. Iwasawa, N. Miyauchi, S. Takagi, Y. Murase, Y. Yamada, A. N. Itakura, and M. Sasaki, Vac. Surf. Sci. **62**, 635 (2019).
[21]N. Miyauchi, T. Iwasawa, Y. Murase, T. Yakabe, M. Kitajima, S. Takagi, T. Akiyama, S. Aoyagi, and A. N. Itakura, Appl. Surf. Sci. **527**, 146710 (2020).
[22]R. Dupuy, M. Haubner, B. Henrist, J. H. Fillion, and V. Baglin, J. Appl. Phys. **128**, 175304 (2020).
[23]H. K. Perkins and T. Noda, J. Nucl. Mater. **71**, 349 (1978).
[24]N. R. Quick and H. H. Johnson, Metall. Mater. Trans. A **10**, 67 (1979).
[25]T. Maeda, S. Naito, M. Yamamoto, M. Mabuchi, and T. Hashino, J. Chem. Soc. Faraday Trans. **24**, 3527 (1998).